(23) Fang, Z.; Zhu, Z.; Zhang, S.; Xu, S.; Guo, L.; Sun, L. *Anal. Chim. Acta* **1988**, *214*, 41-56.
(24) Schulze, G.; Liu, C. Y.; Brodowski, M.; Elsholz, O.; Frenzel, W. *Anal. Chim. Acta* **1988**, *214*, 121-136.
(25) Teder, A. *Sven. Papperstidn.* **1967**, *70*, 197-200.
(26) Schwarzenbach, G. *Pure Appl. Chem.* **1962**, *5*, 377-402.
(27) Giggenbach, W. *Inorg. Chem.* **1972**, *11*, 1201-1207.
(28) Bognar, J.; Jellinek, O. *Anal. Chim. Acta* **1963**, *29*, 395-405.
(29) Koch, W. F. *J. Chromatogr. Sci.* **1989**, *27*, 418-421.
(30) Dasgupta, P. K. In *Ion Chromatography*; Tarter, J. G. Ed.; Marcel-Dekker, New York, 1987; pp 191-367.
(31) van Staden, J. F. *Fresenius' Z. Anal. Chem.* **1982**, *310*, 239-242.
(32) Krug, F. J.; Zagatto, E. A. G.; Reis, B. F.; Bahia, O.; Jacintho, A. O.; Jorgensen, S. S. *Anal. Chim. Acta* **1983**, *145*, 179-187.
(33) Pinkel, D. *Anal. Chem.* **1982**, *54*, 503A-519A.
(34) Zarrin, F.; Dovichi, N. J. *Anal. Chem.* **1985**, *57*, 2690-2692.

RECEIVED for review September 17, 1990. Accepted November 21, 1990. This work was supported by an unrestricted research grant from the Shell Development Co., Houston, TX.

Single-Molecule Detection of Rhodamine 6G in Ethanolic Solutions Using Continuous Wave Laser Excitation

Steven A. Soper,* E. Brooks Shera, John C. Martin, James H. Jett, Jong H. Hahn, Harvey L. Nutter, and Richard A. Keller*

Center for Human Genome Studies, Los Alamos National Laboratory, Los Alamos, New Mexico 87545

The ultimate in analytical sensitivity is the ability to detect analytes on a single-molecule level. Laser-induced fluorescence (LIF) detection of single molecules in solution is hampered by specular, Rayleigh, and Raman scattering that contribute significantly to the background. In order to observe individual fluorescent molecules as they transit the laser beam in the presence of large backgrounds, it is necessary to detect a large number of photons per molecule. One method to increase the number of photons per event is to increase the residence time of the molecule in the laser beam. However, with long residence times, photostability sets an upper limit on the number of times the molecule can be cycled between the ground and first excited singlet state. We have observed the passage of individual rhodamine 6G (R-6G) molecules in ethanol (EtOH). The use of EtOH as a solvent allows one to obtain nearly 2 orders of magnitude more photons per molecule than may be obtained in H_2O. Observation of single molecular events of R-6G in EtOH is substantiated by autocorrelation analysis and from shifts in the histograms of the frequency of photoelectron counts. Results from Monte Carlo simulations also support our experimental results.

INTRODUCTION

The ability to detect individual molecules in flowing sample streams as they transit a focused laser beam with fluorescence detection has important ramifications in the areas of bioanalytical and analytical chemistry. Single-molecule detection (SMD) will be useful in such techniques as fluoroimmunoassays (*1*), various chromatographic analysis such as capillary zone electrophoresis, and flow cytometry. At Los Alamos, we have recently reported on a scheme to sequence DNA at a high rate incorporating single-molecule detection of nucleotides labeled with appropriate fluorogenic tags (*2*, *3*).

Work in the area of single-molecule detection in flowing streams was initiated by Dovichi (*4*) utilizing the 514.5-nm continuous wave (cw) output of an Ar^+ laser and hydrodynamically focused flows of rhodamine 6G (R-6G). Since this work, much progress has been made (*5-8*), and recently evidence for sensitivity at the single-molecule level for phycoerythrin (equivalent to ca. 20 rhodamine molecules based upon the difference in molar absorptivities) has been reported (*9*, *10*). The major obstacle associated with solution SMD is the high background consisting of specular, Rayleigh, and Raman scattering and luminescence from trace impurities in the solvent. This background can be reduced by using time-gated detection. Time discrimination of the background arises from the instantaneous nature of the scattering processes and the relatively long lifetime (typically in the nanosecond regime) associated with the fluorophore. Indeed, we have implemented the use of time-gated detection to observe the passage of individual R-6G molecules in H_2O as they transit a frequency-doubled laser beam from a mode-locked Nd:YAG laser (*11*). The ability to detect single molecules by using cw excitation is inherently more difficult than the time-gated method because of the high background but is instrumentally easier to implement. Therefore, in order to observe the molecular events for cw excitation, it becomes vital to detect as many photons per molecule as possible in order to enhance the signal-to-noise ratio (SNR) in the presence of the large background.

Several different criteria may be used to indicate the passage of a single molecule through the laser beam: (1) observation of the photon burst resulting from the continued cycling of the molecule from the singlet ground state to the first excited singlet state with subsequent decay resulting in fluorescence emission. The cycling process results in photon count rates above the count rate associated with the background. The direct observation of the photon burst resulting from each molecule requires a high SNR, since each event is processed individually. (2) Autocorrelation analysis yielding a nonrandom correlation corresponding to the molecular transit time through the laser beam. The autocorrelation function is sensitive to the number of events and the amplitude of the burst. In addition, the autocorrelation function can give information on the bandwidth of the burst, which is related to the molecular transit time. The autocorrelation function is a sensitive analysis method for single-molecule detection since the entire data string is processed and averaged over a number of events. (3) The presence of high count segments in the histograms of frequency of counts vs counts

* Authors to whom correspondence should be addressed.

0003-2700/91/0363-0432$02.50/0

that are present in the blank predicted from a Poisson distribution fit to the blank only. The distributions are susceptible to noise in the background. The observation of tails in the distributions can be enhanced by summing together the data points associated with one transit time (i.e., over the bandwidth of the signal).

There are a number of instrumental parameters and photophysical constants associated with the molecular species under investigation that should be considered in order to enhance the ability to observe single molecules. For example, increasing the molecular transit time will increase the SNR for single-molecule detection because SNR = $n_f/n_b^{1/2}$, where n_f is the number of detected photons from the molecule and n_b is the detected background counts in one transit time. Properties of the molecule that are important for single-molecule detection are its absorption cross section (σ), fluorescence quantum efficiency (Φ_f), fluorescence lifetime, and photodestruction quantum efficiency (Φ_d). Mathies et al. have shown recently that the photon irradiance and the molecule's photostability both play a crucial role in determining the SNR for single-molecule detection (*12*). They showed that the SNR levels off when the transit time approaches the photodestruction time. Additionally, the SNR for single-molecule detection was shown to approach a limiting value as a function of increasing laser power, resulting from saturation of the electronic transition at high irradiances (*6*, *12*).

We have measured the photostability of R-6G and several other fluorophores in aqueous and ethanolic solutions (*13*). The results of these studies revealed that the photostability of R-6G was nearly 2 orders of magnitude greater in ethanol as compared to water. The importance of this increased photostability in single-molecule detection is that a greater number of photons per molecule may be obtained. The average number of photons that can be realized per molecule (n_T) is given by

$$n_T = \Phi_f/\Phi_d \quad (1)$$

The value of Φ_d for R-6G in EtOH is 5.7×10^{-7}, while in H_2O the value is nearly 2 orders of magnitude larger. In addition, the fluorescence quantum efficiency of R-6G in EtOH (Φ_f = 0.95) is twice that of R-6G in H_2O (*14*, *15*). This results in nearly 2×10^6 photons per molecule (average) that may be obtained from each R-6G molecule in EtOH, while in H_2O only ca. 25 000 photons per molecule (average) are obtainable.

The increased photostability of R-6G in ethanolic solutions was used to observe single molecular events with cw excitation by satisfying two of the three criteria for single-molecule detection. Single-molecule detection was substantiated by the observation of the nonrandom autocorrelation function arising from individual molecules of R-6G and the presence of high count segments in distributions for the number of occurrences vs the counts per interval. These results will be presented in this paper. In addition, Monte Carlo methods were developed, employing the photophysical constants of R-6G, to simulate the passage of individual R-6G molecules through a focused Gaussian laser beam. The results of these simulations, verifying our experimental observations, will also be presented.

EXPERIMENTAL SECTION

The experimental arrangement is shown schematically in Figure 1. The excitation source was a cw Ar^+ laser (Spectra Physics Model 165, Mountain View, CA) operated at 514.5 nm with an average power of ca. 500 mW at the sample. The output power was stabilized by a Coherent Model 28 beam stabilizer (Palo Alto, CA). The polarization of the stabilized output was shifted from vertical to horizontal with a half-wave plate to reduce Rayleigh and Raman scattering contributions to the background. The laser beam was focused into the flow cell with a pair of crossed cylindrical lenses. The $1/e^2$ probe volume dimensions were determined by translating a razor blade across the focused laser beam and measuring the transmitted radiation impinging upon a power meter (Coherent Model 210). The resulting probe volume dimensions were 97 μm (parallel to the flow direction) and 22 μm (perpendicular to the direction of the flow). The elongated probe volume dimension along the flow direction results in long transit times with moderate volumetric flow rates. The resultant irradiance with a cross-sectional area of 2.13×10^{-6} cm^2 and 500 mW was 23.4 kW/cm^2. The fluorescence was collected at right angles with a 40× microscope objective (Model Plan M, NA = 0.55, Nikon INC., Garden City, NY) and focused onto a slit, serving as a spatial filter, to reduce the amount of specular scattered light emanating from the cell walls and impinging upon the phototube. The slit width was set to 200 μm, resulting in an observation distance of 5 μm along the propagation axis of the laser beam. The resultant probe volume, defined by the $1/e^2$ intensity of the laser beam and the image of the slit on the sample stream, was 10.7 pL.

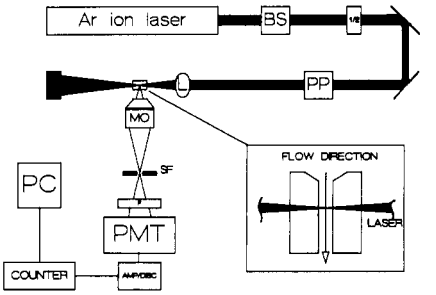

Figure 1. Schematic of the cw single-molecule detection apparatus. BS = laser power stabilizer, 1/2 = half wave plate, PP = polarizing prism, L = lens (focal length = 5 cm), MO = microscope objective (40X, NA = 0.55), SF = spatial filter, F = fluorescence band-pass filter, Amp/Disc = amplifier and discriminator, PC = PDP 11 microcomputer. The insert shows a cross-sectional view of the Ortho flow cell.

The fluorescence emission and scattered light were filtered with a wide band-pass filter (Omega Optical, Brattleboro, VT) centered at 560 nm and a width of 40 nm (FWHM). The absorbance of the filter is ca. 6 at 514.5 nm with a transmission efficiency of ca. 80% at 560 nm. The phototube was an RCA Model 31034A photomultiplier (quantum yield ca. 0.24 at 550 nm) with the individual photon events detected via an EG&G amplifier/discriminator (Model 1121A, Princeton, NJ). The detected pulses were recorded in programmed bin widths (100–400 μs) on a Joerger Model S3 counter (East Northport, NY) interfaced to a PDP 11 microcomputer. All data analysis software was written in Turbo Pascal Version 5.5 (Borland, Scotts Valley, CA). The flow cell was an Ortho flow cytometer cell (Model 300-5035-000, Becton Dickinson, East Rutherford, NJ) and is shown diagrammatically in the insert of Figure 1. The quartz cell has a square bore with a cross-sectional area of 6.25×10^{-4} cm^2. In the present experiments, hydrodynamically focused flows were not used. Without focused flows, a significant number of sample molecules do not pass through the probe volume, but the intent of these experiments was to observe the burst only from those molecules that do pass through the probe volume. Solutions were delivered to the cell with a Harvard Model 22 syringe infusion pump (South Natick, MA).

R-6G was obtained from Exciton (Dayton, OH) and used as received. Solvents were spectral grade and obtained from Burdick & Jackson (Muskegon, MI). EtOH solvents were screened carefully, since it was observed that the background varied from bottle to bottle. The concentration of R-6G used in all experiments was adjusted such that the probability of a single R-6G molecule residing within the probe volume at any given time was ca. 0.05 (ca. 10^{-14} M), making the probability of two R-6G molecules within the probe volume at any one time ca. 0.0025.

Simulation programs, written in Turbo Pascal, were used to model the passage of individual molecules through a focused Gaussian laser beam. The background was generated with random numbers that were constrained to follow a Poisson distribution. Molecules were placed randomly in the simulated data string. The number of photons per molecule per transit was based upon the peak laser irradiance (I_p in photons cm^{-2} s^{-1}), the position the

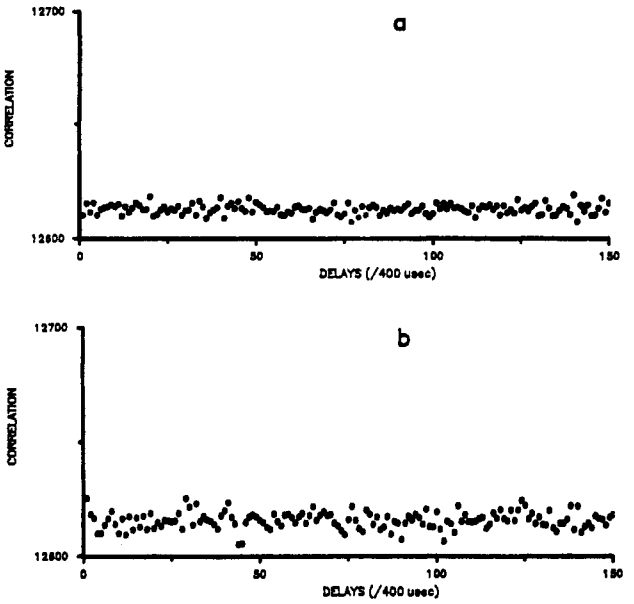

Figure 2. (a) Experimental autocorrelation analysis for the passage of R-6G molecules through a focused Gaussian laser beam (probe volume = 10.7 pL) in a solvent of H_2O. Experimental parameters were as follows: laser power = 500 mW, transit time = 2 ms, probability of molecule in probe volume = 0.05, Φ_f = 0.45, $\Phi_d = 1.8 \times 10^{-5}$, and $\sigma = 2.4 \times 10^{-16}$ cm^2/molecule. The channel size was 100 μs and the data were binned in groups of 4 prior to performing the autocorrelation, yielding 5 points per transit. (b) Autocorrelation for simulated results of R-6G in H_2O. The experimental parameters were those used as in Figure 2a and an instrumental conversion efficiency of 0.0015 photoelectron per emitted photon, where the conversion efficiency is a sum of the geometric collection efficiency, the throughput of the band-pass filter for R-6G fluorescence, and the quantum efficiency of the phototube at the monitored wavelengths.

molecule travels through the probe volume, the photophysical constants of the molecule (σ, Φ_f, and Φ_d), and the measured collection efficiency of the instrument (0.0015 photoelectron/photon).

RESULTS AND DISCUSSION

One criterion that has been used as evidence for single-molecule detection is the observation of a nonrandom correlation in the data corresponding to the molecular transit time (*10*). Because of the random nature of the background, autocorrelation analysis of these data should yield no such correlation. When molecules transit the laser beam, a characteristic bandwidth corresponding to the molecular transit time is generated resulting from the correlated photon burst. The expression for the autocorrelation function is given in the Appendix (eq 1A). The magnitude of the nonrandom autocorrelation function is proportional to the square of the amplitude of the photon burst when the background is small compared to the signal. When the background is slightly larger than the amplitude of the burst, the magnitude of the correlation is directly related to the burst size. In the case where the background counts are much greater than the counts resulting from the burst, no observable nonrandom correlation is seen (Appendix). Therefore, in order to observe a nonrandom correlation in the data associated with the transit time, it is imperative that most of the molecules transit the entire length of the probe volume, generating a large number of photons.

The experimental and simulated results of an autocorrelation analysis for R-6G in H_2O are presented in Figure 2. The simulation employed the same parameters used for the experimental data shown in Figure 2a along with the measured photophysical constants of R-6G in H_2O. As is evident from these results, no nonrandom correlation corresponding to the molecular transit time is observed in this solvent.

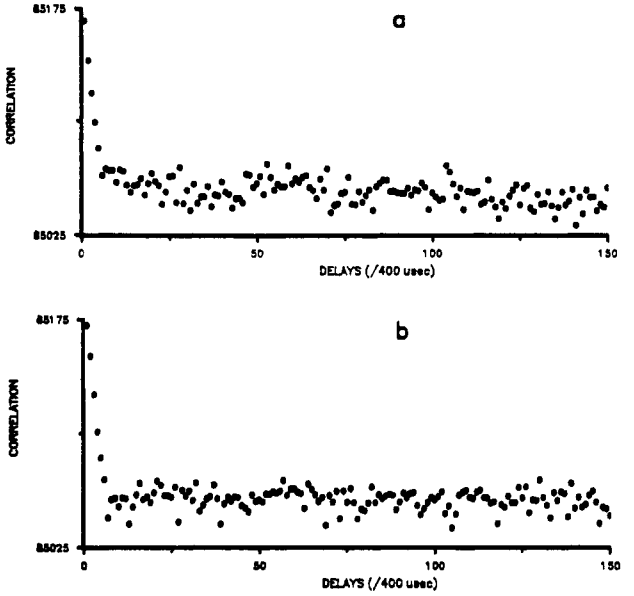

Figure 3. (a) Autocorrelation analysis of experimental data for the passage of R-6G molecules through a focused Gaussian laser beam in an EtOH solvent. The experimental parameters used were as follows: laser power = 500 mW, transit time = 2 ms, Φ_f = 0.95, probability of molecule in probe volume = 0.05, $\Phi_d = 5.7 \times 10^{-7}$, $\sigma = 2.4 \times 10^{-16}$ cm^2/molecule, and probe volume = 10.7 pL. The channel size was 100 μs, and the data were grouped in bins of 4 before performing the autocorrelation, corresponding to 5 points per transit. (b) Autocorrelation for simulated data of R-6G in EtOH. The same simulation parameters were used as those of Figure 2b except for substitution of the appropriate values of Φ_f and Φ_d for R-6G in EtOH.

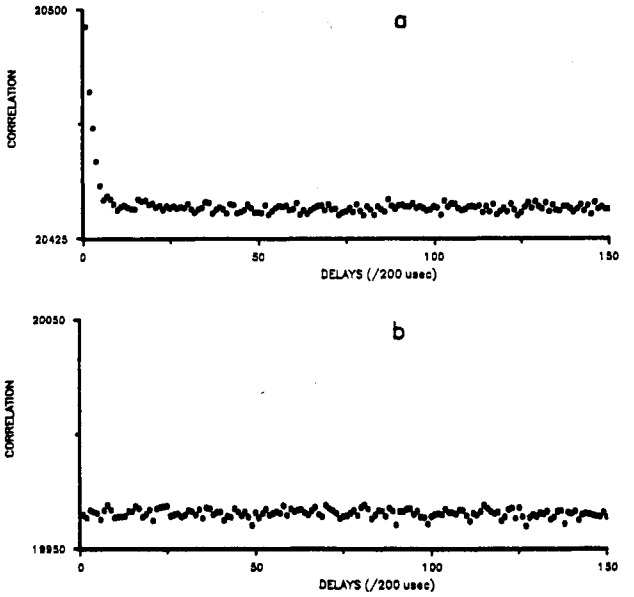

Figure 4. (a) Experimental autocorrelation function for R-6G in EtOH traveling through a Gaussian laser beam with a transit time of 1 ms. The parameters of the experiment were identical with those used for the data of Figure 3a. (b) The autocorrelation function of EtOH only.

The experimental and simulated results of an autocorrelation analysis for R-6G in EtOH are presented in Figure 3. The simulation employed the same parameters used for the simulation shown in Figure 2 incorporating the photophysical constants of R-6G in EtOH. As is evident from Figure 3a, a nonrandom correlation is observed from the experimental data, with the correlation corresponding to the molecular transit time of 2 ms. This correlation is good evidence for the observation of bursts of photons from individual R-6G molecules transiting the Gaussian laser beam. In Figure 4, the flow velocity was increased by a factor of 2, reducing the transit

time to 1 ms. As can be seen from this figure, the correlation runs to delays of 1 ms, consistent with the calculated 1-ms transit time. Figure 4b shows the autocorrelation function for EtOH in the absence of R-6G. In this case, no nonrandom correlation is seen.

The magnitude of the nonrandom autocorrelation (g_{nr}) shown in Figure 3a, extrapolated to $\tau = 0$, is ca. 112, calculated from 80 000 data points where the average number of background counts per 4 data points is equal to 196 counts. The number of events (N_{ev}) can be calculated from the probability of a molecule residing in the probe volume at any given time interval ($P = 0.05$), the molecular transit time ($t = 2$ ms), the time width of each data point ($T_d = 100\ \mu s$), and the number of data points ($N = 80\,000$) by using the following equation:

$$N_{ev} = PNT_d/t \qquad (2)$$

From eq 2, the calculated number of events is 200. The application of eq 8A from the Appendix to the data of Figure 3a yields ca. 114 detected photons per molecule. The number of photons per molecule from the simulated data used to construct the plot of Figure 3b was 120, in good agreement to the experimental value obtained from the autocorrelation function shown in Figure 3a. The SNR for single-molecule detection of R-6G in EtOH with a transit time of 2 ms is $114/(980)^{1/2}$ or 3.64.

The presence of a nonrandom correlation for R-6G in EtOH and the absence of such a correlation in H_2O can be explained by two factors associated with the increased photon yields of R-6G on a molecular basis in EtOH as compared to H_2O: (1) The fluorescence quantum yield is nearly 2 times greater in EtOH (*14*, *15*). (2) The quantum yield for photodestruction of R-6G in EtOH is ca. 2 orders of magnitude smaller than that of R-6G in H_2O (*13*). Indeed, these were the only two parameters that were altered in the simulated results shown in Figures 2b and 3b. The lack of a nonrandom correlation in the case of H_2O indicates that only a few photons per molecule are obtainable. In this case, the background counts in one transit time are much greater than the photons detected per molecule. The results of the simulation for R-6G molecules in H_2O and a transit time of 2 ms yielded ca. 15 detected photons per molecule. The experimentally determined background counts associated with this time interval were 205 counts. The resulting SNR under these conditions is 1.05 (*8*).

The probability of photodestruction (P_d) can be expressed as

$$P_d = \sigma I_{x,y} \Phi_d t \qquad (3)$$

where $I_{x,y}$ is the photon flux of the Gaussian laser beam at coordinates (x,y) within the probe volume, σ is the absorption cross section, and t is the time the molecule spends in the laser beam at coordinates (x,y). The result is an exponential decay of the number of unbleached molecules as a function of the number of excitations they experience. The implications of this expression are 2-fold: (1) The further the molecule travels into the probe volume up to the central region, the greater the probability for photodestruction due to the increase in the laser intensity because of the Gaussian nature of the beam. (2) The molecule possesses a finite probability of being photobleached after only a few excitations. Therefore, as the Φ_d becomes larger (decreased photostability), the probability for missing molecular events increases because of the low number of photons some molecules will emit and thus escape detection.

The second criterion used to verify detection of single molecules is the observation of skewed distributions (number of occurrences of a particular count rate vs count rate) in the presence of the fluorophore as compared to the background distribution of the solvent only. A tail on the high count side of the distribution results from the photons arising from individual molecules as they transit the laser beam. The distributions of the background (EtOH only) and R-6G (in EtOH) with a transit time of 2.0 ms are shown in Figure 5. Since each data point consists of counts integrated over a 100-μs time interval, yielding 20 data points per transit, the data from 20 consecutive points were summed to represent the photons emitted by each molecule during one transit. As can be seen from Figure 5, the distribution with R-6G gives a higher number of occurrences above ca. 1070 counts. To show this tail more clearly, the difference distribution (R-6G + background − background) is shown as the insert in Figure 5. The difference distribution demonstrates the increase in the number of occurrences in the high count rate portion of the distribution. The counts associated with the peak in the difference distribution (P_{dd}) can be related to the average number of photons per molecule by

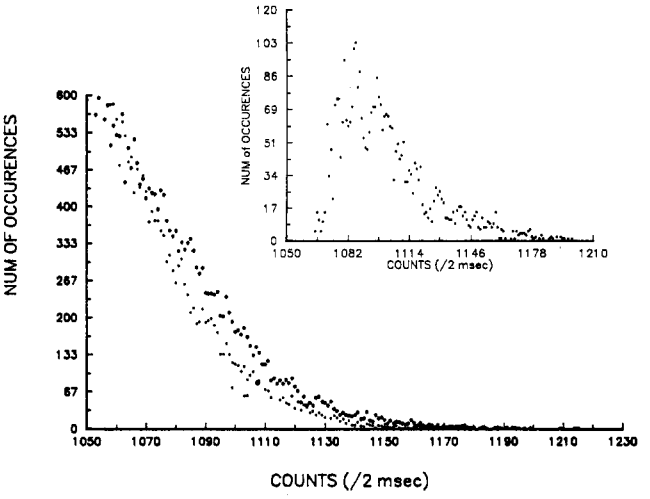

Figure 5. Sliding sum distribution for ca. 200 molecular events of R-6G molecules transiting the laser beam with a transit time of 2 ms and an EtOH solvent. The distributions of the blank (dots) and R-6G (closed circles) were subjected to a 20-point sliding sum with the same data used in the analysis as that used in the plot of Figure 3a. The insert shows the difference distribution.

$$P_{dd} = B_{ave} + N_{ave} \qquad (4)$$

where B_{ave} is the average number of background counts per transit time and N_{ave} is the average number of photons per molecule per transit. Taking $P_{dd} = 1088$ (from inset of Figure 5) and $B_{ave} = 980$, a value of 108 is obtained for N_{ave}, in good agreement to the value of 114 obtained from the autocorrelation functions for R-6G in ethanol.

The total number of events as calculated with eq 2 and a 2-ms transit time was found to be ca. 200. Integration of the difference distribution of Figure 5 and dividing this result by the number of events result in ca. 17 occurrences per event. Performing a 20-point sliding sum distribution on the simulated data used to construct the plot of Figure 3b and subtracting simulated background data, the number of occurrences per event was found to be ca. 16, in excellent agreement with the experimental result. The large number of occurrences per event arises from the fact that in sorting the data each event is counted more than once. The number of times each event is actually counted depends upon the number of photons that are detected per molecule and the magnitude of the background count rate surrounding each event.

We were unable to observe the actual photon burst above the background from R-6G molecules even with transit times approaching 8 ms in H_2O or EtOH. The poor photostability of R-6G molecules in H_2O eliminates the possibility of using extended transit times with moderate laser irradiances since the majority of the molecules are photobleached within the first few milliseconds. In fact, extending the transit time much beyond the average time the molecule can spend in the beam

before being photobleached decreases the SNR for single-molecule detection since the number of photons per molecule does not increase, but the background counts accumulated in one transit time actually increases. The advantage of using H_2O as a solvent in cw systems is that the only Raman band that falls within the fluorescence observation window is the 1650-cm^{-1} O–H bending vibration, which possesses a very small cross section (*3*, *13*, *14*). In the case of EtOH, although the photon yield per molecule is greater than that for H_2O, the background is considerably higher (ca. 5 times higher in the case of EtOH as compared to H_2O).

CONCLUSION

The ability to detect single molecules in flowing sample streams is dependent upon a number of instrumental parameters and photophysical constants associated with the molecule under investigation. Many elaborate optical methods have been proposed to improve the optical collection efficiency for SMD (*16–18*). When increasing the geometric collection efficiency, the background goes up as well as the signal and the net increase in the SNR is the square root of the improvement in the collection efficiency factor. Another approach is to address the photophysical constants of the molecule under investigation. Of the photophysical constants associated with the molecule, the molecular photostability is the property that may, in some cases, be successfully manipulated by the proper choice of the solvent. For R-6G, switching the solvent from H_2O to EtOH results in nearly 2 orders of magnitude more photons per molecule. A possible alternative to altering the nature of the solvent is to purge the system of dissolved O_2 in order to enhance the photostability of the molecule under investigation.

We have demonstrated that two of the three criteria used in verifying single-molecule detection have been observed for R-6G in ethanolic solutions. Autocorrelation analysis was employed as a means to demonstrate the presence of the correlated photon bursts from molecules traveling through the laser beam. The results presented herein demonstrate our ability to observe correlated bursts from R-6G molecules in EtOH. The inability to observe the correlated bursts in H_2O is a direct result of the low photon yield per molecule, a consequence of the poor photostability and low fluorescence quantum yield of R-6G in H_2O.

The second criterion that is used to give conformation of single-molecule detection is the observation of tails in the distributions of number of occurrences vs counts per time interval. This results from the increased occurrence of high counting rates produced by molecules transiting the laser beam. Our results have shown such tails in the distribution when R-6G is added to EtOH.

APPENDIX

For discretely sampled data, the autocorrelation function ($G(\tau)$) can be written as

$$G(\tau) = 1/N\sum_{t=0}^{N-1} h(t)\ h(t+\tau) \qquad (1A)$$

where N is the number of data points included in the calculation and is used to normalize the autocorrelation function, $h(t)$ is a data point at time (t), and $h(t+\tau)$ is a data point at a certain delay time (τ). The autocorrelation function is composed of random (g_r) and nonrandom (g_{nr}) correlations ($G(\tau) = g_{nr} + g_r$). The one of interest in the SMD is the nonrandom correlation, arising from the correlated burst of photons from molecules traversing the laser beam. The observed duration of these correlated bursts should correspond to delay times up to the molecular transit time.

The autocorrelation function can be rewritten, assuming a "flat top" response, in terms of the amplitude of the photon burst (S) and the integrated background counts over the time duration of the data point (b) at $\tau = 0$ by the following relationship:

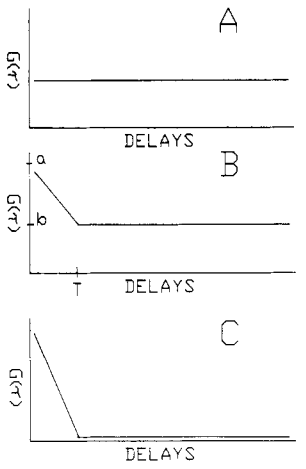

Figure 6. Autocorrelation functions for three cases of the relation between the photon burst amplitude (S) and the magnitude of the background (b). (A) Case 1, $S \ll b$. (B) Case 2, $S < b$. Point a is the extrapolated $\tau = 0$ point where $G(\tau=0) = g_r + g_{nr}$, point b is the extrapolated $\tau = 0$ point where $G(\tau=0) = g_r$, and point T is the molecular transit time. (C) Case 3, $S > B$.

$$G(\tau=0) = 1/N\sum_{t=0}^{N-1}(S_t + b_t)^2 \qquad (2A)$$

Expanding eq 2A leads to

$$G(\tau=0) = 1/N\sum_{t=0}^{N-1}(S_t^2 + 2S_tb_t + b_t^2) \qquad (3A)$$

Three cases can be considered with regard to eq 3A and are shown in Figure 6. In the first case (Figure 6A), $S \ll b$, and eq 3A becomes

$$G(\tau=0) = g_r = 1/N\sum_{t=0}^{N-1} b_t^2 \qquad (4A)$$

In this case, no nonrandom correlation is observed because the amplitude of the burst is much smaller than the background count rate.

The next case results when $S < b$ (see Figure 6B), and eq 3A can be rewritten as

$$G(\tau=0) = g_r + g_{nr} = 1/N\sum_{t=0}^{N-1}(2S_tb_t + b_t^2) \qquad (5A)$$

The random contribution (g_r) can be written as in eq 4A, and the nonrandom contribution (g_{nr}) can be expressed as

$$g_{nr} = 1/N\sum_{t'=1}^{N_{ev}T_b} 2S_{t'}b_{t'} \qquad (6A)$$

where N_{ev} is the number of events and T_b is the duration of the burst (number of data points per burst). The summation in this case is performed only over the events. As can be seen, the autocorrelation function is directly related to the amplitude of the burst.

In the last case, $S \gg b$ (Figure 6C), eq 3A becomes (neglecting the random contribution and performing the sum only over the number of events)

$$g_{nr} = 1/N\sum_{t'=1}^{N_{ev}T_b} S_{t'}^2 \qquad (7A)$$

In this case, the autocorrelation function is related to the square of the amplitude of the photon burst.

Performing the summation from eq 6A over the number of events and solving for ST_b (the number of detected photons

per molecule per transit time), one obtains

$$ST_b = \frac{g_{nr}N}{2N_{ev}b} \quad (8A)$$

The value taken for g_{nr} at $\tau = 0$ is that arrived at by extrapolating the autocorrelation function at $\tau > 0$ to $\tau = 0$ (see Figure 6) and subtracting the average background level (g_r). The values for S and b are taken as the average values. As can be seen from eq 8A, the number of photons per molecule per transit time can be calculated from the magnitude of the autocorrelation function at the extrapolated $\tau = 0$ value when $S < b$.

LITERATURE CITED

(1) Saunders, G. C.; Jett, J. H.; Martin, J. C. *Clin. Chem.* **1985**, *31*, 2020.
(2) Jett, J. H.; Keller, R. A.; Martin, J. C.; Marrone, B. L.; Moyzis, R. K.; Ratliff, R. L.; Seitzinger, N. K.; Shera, E. B.; Stewart, C. C. *J. Biomol. Struct. Dyn.* **1989**, *7*, 301.
(3) Davis, L. M.; Fairfield, F. R.; Jett, J. H.; Keller, R. A.; Hahn, J. H.; Krakowski, L. A.; Marrone, B. L.; Martin, J. C.; Ratliff, R. L.; Shera, E. B.; Soper, S. A. *Genet. Anal.*, in press.
(4) Dovichi, N. J.; Martin, J. C.; Jett, J. H.; Trkula, M.; Keller, R. A. *Anal. Chem.* **1984**, *56*, 348.
(5) Dovichi, N. J.; Martin, J. C.; Jett, J. H.; Keller, R. A. *Science* **1983**, *219*, 845.
(6) Nguyen, D. C.; Keller, R. A.; Trkula, M. *J. Opt. Soc. Am.* **1987**, *4*, 138.
(7) Jett, J. H.; Keller, R. A.; Martin, J. C.; Nguyen, D. C.; Saunders, G. C. *Flow Cytometry and Sorting*; Wiley-Liss: New York, 1990; pp 381-396.
(8) Hahn, J. H.; Soper S. A.; Nutter, H. L.; Martin, J. C.; Jett, J. H.; Keller, R. A. *Appl. Spectrosc.*, in press.
(9) Nguyen, D. C.; Keller, R. A.; Jett, J. H.; Martin, J. C. *Anal. Chem.* **1987**, *59*, 2158.
(10) Peck, K.; Stryer, L.; Glazer, A. N.; Mathies, R. A. *Proc. Natl. Acad. Sci. U.S.A.* **1989**, *86*, 4087.
(11) Shera, E. B.; Seitzinger, N. K.; Davis, L.; Keller, R. A.; Soper, S. A. *Chem. Phys. Lett.* **1990**, *174*, 553.
(12) Mathies, R. A.; Peck, K.; Stryer, L. *Anal. Chem.* **1990**, *62*, 1786.
(13) Soper, S. A.; Davis, L. M.; Jett, J. H.; Martin, J. C.; Nutter, H. L.; Shera, E. B.; Keller, R. A. Manuscript in preparation.
(14) Alfano, R. R.; Shapiro, S. L.; Yu, W. *Opt. Commun.* **1973**, *7*, 191.
(15) Kubin, R. F.; Fletcher, A. N. *J. Lumin.* **1982**, *27*, 455.
(16) Skogen-Hagenson, M. J.; Salzman, G. C.; Mullaney, P. F.; Brockman, W. H. *J. Histochem. Cytochem.* **1977**, *25*, 784.
(17) Watson, J. V. *Br. J. Cancer* **1985**, *51*, 433.
(18) Watson, J. V. *Cytometry* **1989**, *10*, 681.

RECEIVED for review September 11, 1990. Accepted December 13, 1990.

Determination of Purine Bases by Reversed-Phase High-Performance Liquid Chromatography Using Real-Time Surface-Enhanced Raman Spectroscopy

Rongsheng Sheng

Center of Analysis and Measurement, Wuhan University, Wuhan, Hubei, People's Republic of China

Fan Ni

Diagnostics Laboratory of Veterinary College, Iowa State University, Ames, Iowa 50011

Therese M. Cotton*

Department of Chemistry, Iowa State University, Ames, Iowa 50011

The determination of four purine bases (adenine, guanine, hypoxanthine, and xanthine) by reversed-phase high-performance liquid chromatography (RP-HPLC), in combination with real-time surface-enhanced Raman spectroscopy (SERS) detection, is demonstrated. The goal of this study was to examine several factors (laser irradiation, pH, memory effects, and the construction of the interface between the RP-HPLC system and the Raman spectrometer) that affect SERS detection under flowing conditions. The separation and detection of a mixture of four purine bases was accomplished. The quantity of bases used for the analysis was 1 mmol for adenine and guanine, 5 nmol for xanthine, and 10 nmol for hypoxanthine. Three-dimensional (SERS intensity, Raman shift, and chromatographic retention time) and two-dimensional (SERS intensity and chromatographic retention time) chromatograms are presented.

INTRODUCTION

The detection and quantitation of nucleotides, nucleosides, and their bases has become increasingly important in the field of biomedical research. The presence of nucleic acid components in physiological fluids, tissues, and cells results from catabolism of nucleic acid, enzymatic degradation of tissues, dietary habits, and various salvage pathways. Changes in the concentration of these components may reflect substantial alterations in the activity of catabolic, anabolic, and interconversion enzymes and may be used to indicate the presence of various disease states which cause alterations in the normal purine and pyrimidine metabolic pathways. At present, high-performance liquid chromatography (HPLC) is considered the most promising method for the determination of purine and pyrimidine metabolites. It is also a powerful technique for monitoring the therapeutic response to purine- and pyrimidine-based drugs and for determination of their effectiveness and toxicity (*1-3*).

Although analysis of nucleic acid components can now be achieved rapidly, accurately, and with high sensitivity by HPLC, the assignment of individual peaks in highly populated chromatograms remains a major problem. Retention times are not sufficient for positive identification of separated components, unless additional information is available. Ultraviolet (UV) spectroscopy has been widely used for this purpose, but the spectra are often difficult to assign unambiguously, especially when closely related or difficult to sep-

* Author to whom correspondence should be addressed.

0003-2700/91/0363-0437$02.50/0